A WAVELET TRANSFORM APPLIED TO ACOUSTIC EMISSION SIGNALS: PART 1: SOURCE IDENTIFICATION [#]

M. A. HAMSTAD[+], A. O'GALLAGHER and J. GARY

National Institute of Standards and Technology, Materials Reliability Division (853), Boulder, CO 80305-3328;
[+]Also Department of Engineering, University of Denver, Denver, CO 80208.

Abstract

A database of wideband acoustic emission (AE) modeled signals was used in Part 1 to examine the application of a wavelet transform (WT) to identify AE sources. The AE signals in the database were created by use of a validated three-dimensional finite element code. These signals represented the out-of-plane displacements from buried dipole sources in aluminum plates 4.7 mm thick and of small and large lateral dimensions. The surface displacement signals at three far-field distances were filtered with a 40 kHz high-pass filter prior to applying the WT. The WTs were calculated with AGU-Vallen Wavelet, a freeware software program. The effects of propagation distance, AE source type, and the depth of the AE source below the plate surface were examined. Specifically, a ratio of the WT magnitude (WT coefficient) from the fundamental anti-symmetric mode to that from the fundamental symmetric mode was studied for correlation with the AE source type. The WT magnitudes were those corresponding to a particular group velocity and signal frequency for each mode. For sources in the large plate located at the same depth, the ratios were able to distinguish different source types and exhibited only small changes with increasing propagation distance. But, when the variable of depth of the source was introduced, the ratios did not uniquely classify the AE source type. In the case of the small coupon plate specimen, reflections from the specimen edges distorted and complicated the WTs. Since the current coupon database excludes (except for one case) the parameter of changes in the distance of the source from the coupon sides, a full examination of these complications was not possible.

1. Introduction

Since early in the history of AE, a goal of AE practitioners has been to use AE signals as the means to identify the type of source that generated the signals (Mehan and Mullin, 1971). Papers have been published indicating the successful identification of AE sources, and commercial AE companies offer software for the purpose of identifying AE sources. These efforts are often controversial because they lack an analytical justification (based on the theory of AE) of the signal features used to sort the experimental signals into different types of sources. Alternatively, some AE source-identification experiments have been carried out with specimen geometries and sensor locations such that signals are obtained from the direct longitudinal bulk waves in several directions of radiation (Buttle and Scruby, 1990a). The analysis that is used to sort these signals into different source types (or combinations of source types) is based on analytical calculations (forward modeling) that determine the relative amplitudes of the first bulk longitudinal signals in different radiation directions. By comparing relative experimental bulk wave amplitudes in different directions with the calculated results for a series of possible sources, the experimental

---

[#] Contribution of the U.S. National Institute of Standards and Technology; not subject to copyright in the US.

sources were identified in a more satisfying fashion. However, in many AE applications Lamb waves are present due to plate-like test specimens and observation of the AE signals in the far-field. In this case, this more satisfying approach is not directly applicable. Some AE researchers (Weaver and Pao, 1982a, b; Guo et al., 1998) have presented analytical results (forward modeling) for Lamb waves in infinite plates, but to date they have not published an extensive database that could lead to source identification of experimental signals by appropriate comparisons.

The AE source-identification research presented here uses an extensive database of modeled Lamb-wave AE signals. These signals were obtained by use of a validated finite-element modeling code (Hamstad et al., 1999). Since the exact source type and all its characteristics are known for each signal, the features of the AE signals can be unequivocally associated with particular source types. In the case of experimental signals, this is not the case. In this paper we examine the possibilities of extracting meaningful source identification features by the use of a wavelet transform (WT). To retain the possibility of a direct method of source identification (rather that an artificial-intelligence method), this paper examines the extraction of limited data sets from the WT results. In addition, if the direct method is not completely successful, these results could provide insight into the most relevant WT results to input into an artificial-intelligence approach.

2. Description of AE Database

The AE signals that comprised the analyzed database were all calculated by the NIST- Boulder finite-element modeling (FEM) code. This code has been validated (Hamstad et al., 1999; Prosser et al., 1999) for buried dipole-type point sources operating in plate specimens with infinite lateral dimensions and for surface and edge monopole sources on plates with small and large lateral dimensions. The specimen domains in the database were aluminum plates 4.7 mm thick. These plates had lateral dimensions of either 1000 mm by 1000 mm (representing the infinite-plate case) or 480 mm by 25.4 mm (representing a small coupon specimen). Figure 1 shows a drawing of the small specimen superimposed on the large specimen. The lateral position of the AE source and the positions where the plate top surface out-of-plane displacement was determined as a function of time are shown. These displacement signals provide the AE signals that would be obtained in a single direction of radiation (toward sensors 1, 2 and 3) or the opposite direction (toward sensors 5, 6, and 7). All the sensor positions were 60 mm apart.

The calculated signals provided a unique and ideal database that was far superior to experimental AE signals for the study of AE source identification. The reasons for this superiority are due to exact knowledge of key information not always available in experimental data: point-source location in three dimensions; source rise time; magnitude and orientation of source dipoles; absolute out-of-plane displacement of a perfect wideband point sensor at an exact location; known filtering of the AE signal; signals both with specimen edge reflections and without such reflections; and signals that are largely free of noise.

For this study of AE source identification, the analyzed database included three types of buried point-sources: (1) in-plane dipole, aligned with the propagation direction to the sensors, (2) out-of-plane dipole, and (3) crack initiation (three dipoles) with the largest dipole aligned with the propagation direction to the sensors. The dipole forces (body forces) were all 1 N except for the two smaller dipoles in the microcrack case, which were 0.52 N (based on the elastic constants of aluminum). Each dipole was made up of a "central" cell having no body force, along with single cells on each side of the "central" cell having body forces. All the
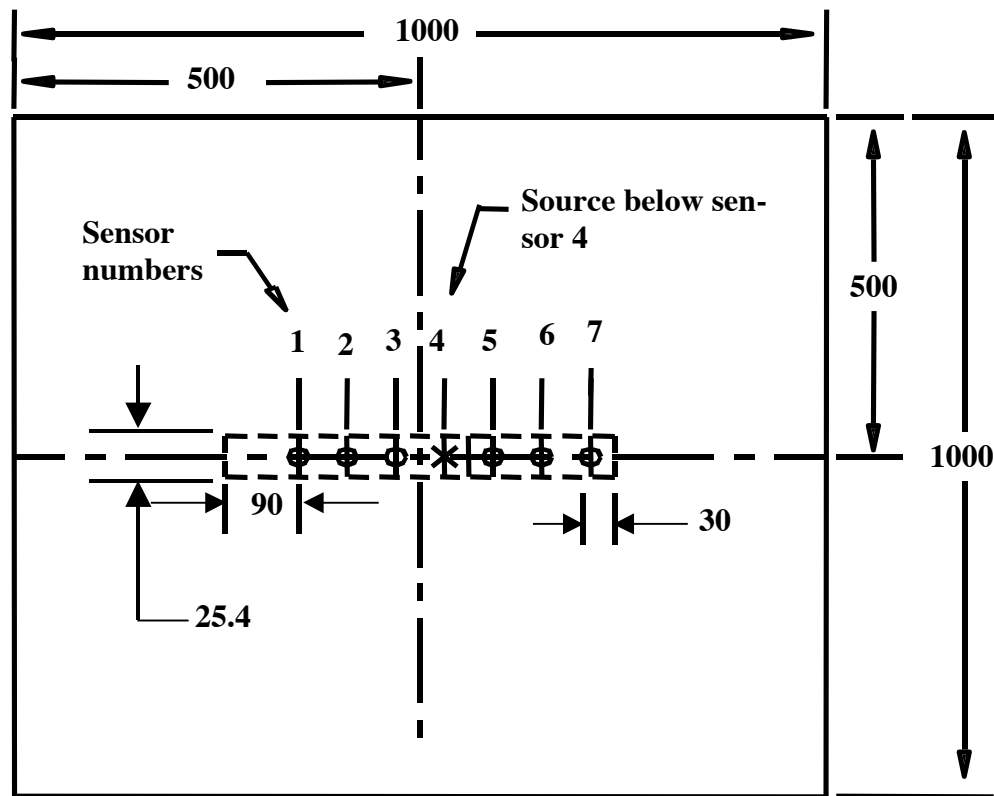
Fig. 1 Large specimen with superimposed small coupon specimen. Sensor positions, spaced 60 mm apart, show points where out-of-plane displacement was determined versus time. All dimensions in mm.

calculations were based on a uniform three-dimensional cell size of 0.313 mm, which was chosen to conform to the requirements for convergence (Hamstad et al., 1999). For the examination of propagation distance, the database included three propagation distances (60, 120, and 180 mm). The three distances were all in the far-field for the 4.7 mm thick plate. In addition, the database included the very important (as will be seen below) variable of depth of the point source below the top surface of the plate. All the sources had a rise time (of the dipole) of 1.5 μs with a "cosine bell" temporal dependence (Hamstad et al., 1999). This rise time resulted in AE signals with frequencies up to about 1 MHz (as determined from spectra calculated by a Fast Fourier Transform (FFT)). To provide a realistic database, all the AE signals were filtered with a 40 kHz high-pass four-pole Butterworth filter prior to analysis. Also, to represent experimental practice, all the calculated digital signals were resampled to a time step of 0.1 μs from the original calculation time step of 0.045 μs. Comparisons demonstrated that this resampling had no apparent effect on the waveforms or their FFTs. The calculated total signal length in each case was 200 μs beginning from the start of operation of the AE source.

3. General Examination of WT Results

Figure 2 shows an example of an AE signal without edge reflections and its calculated WT magnitude (WT coefficients) as a function of frequency versus time. The source for this signal was an in-plane dipole centered at a depth of 1.723 mm (the center of the "central" cell) below the plate top surface. The signal represents the top-surface out-of-plane displacement at 180 mm from the epicenter of the source. All the WTs were calculated with AGU-Vallen Wavelet, a freeware software program (Vallen-Systeme GmbH, 2001; H. Suzuki et al., 1996). AGU-Vallen
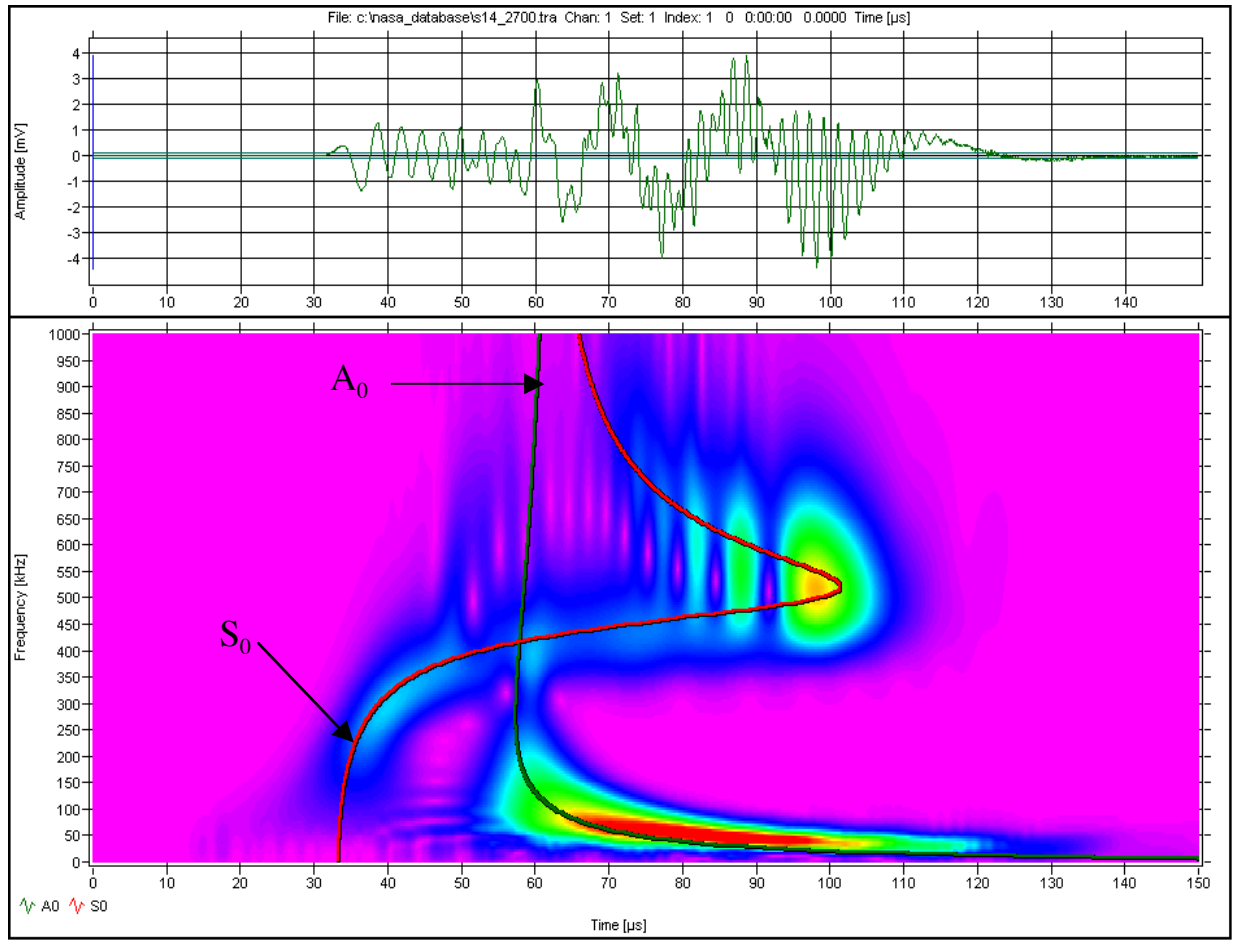
Fig. 2   Typical calculated AE signal from an in-plane dipole source with corresponding WT. Superimposed fundamental symmetric, So, and anti-symmetric, Ao, modes after converting group velocity to time based on 180 mm propagation distance. Red color corresponds to highest magnitude of the WT. Source depth is 1.723 mm in large specimen. (WT scale: 1 MHz: 150 μs)

Wavelet has been developed in collaboration between Vallen-Systeme GmbH and Aoyama Gakuin University (AGU), Tokyo, Japan. The AGU group has pioneered in the research of wavelet analysis in the field of acoustic emission (Suzuki et al., 1996; Takemoto et al., 2000; Yamada et al., 2000). This program has a Gabor function as the "mother" wavelet with a central frequency of 7 MHz. The software program also includes a program to calculate the relevant group-velocity curves for the lowest ten modes of the infinite number of Lamb modes that govern the far-field wave propagation in a plate. Figure 2 shows the two lowest modes (fundamental symmetric, So, and anti-symmetric, Ao) superimposed on the WT. This superposition is facilitated by an option that converts the group velocity scale to a time scale using the known exact propagation distance. The group-velocity curves were calculated by use of the same bulk velocities that were used in the finite-element computations (6,320 m/s bulk longitudinal velocity and 3,100 m/s bulk shear velocity). The FEM calculation also uses the material density of 2700 kg/m^3. The color scale in Fig. 2 is a linear scale with red representing the highest-magnitude region of the WT and pink the smallest or zero-magnitude region. The display includes an option to change the color scale (called the color factor) so as to include a greater or lesser portion of the maximum magnitudes in the "red" region. The WT in Fig. 2 has a color-factor (CF) value of 0.8. A color factor of less than 1 (the default value) means that a wider range of the WT peak magnitudes are displayed in red. The converse applies for color factors greater than 1.
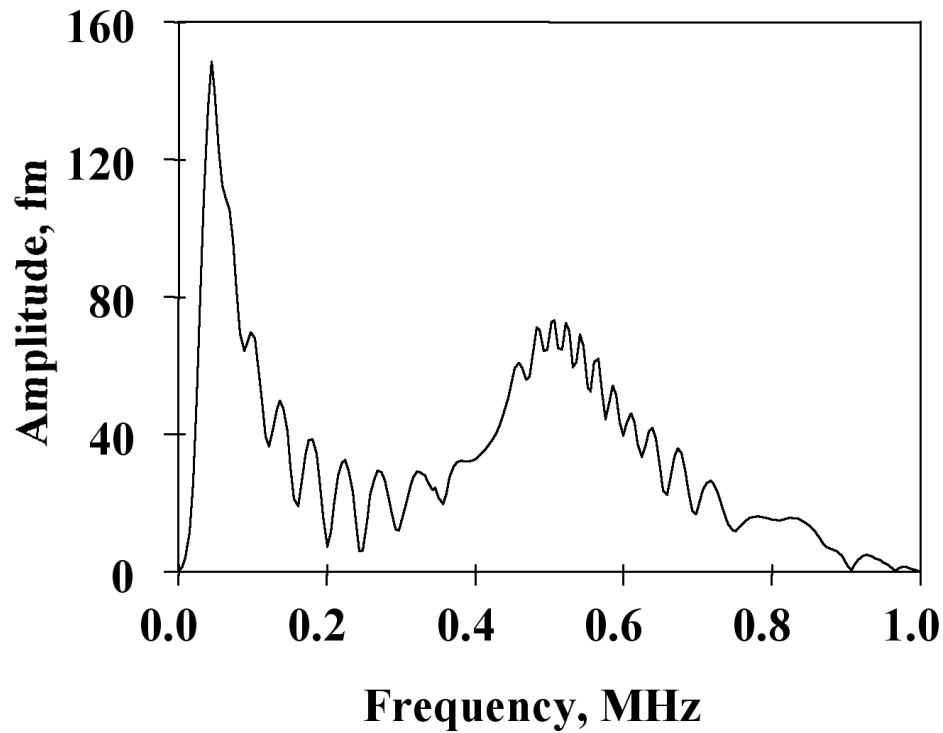
Fig. 3 FFT of the waveform shown in Fig. 2.

Clearly, Fig. 2 shows the presence of AE signal energy in portions of both the fundamental symmetric and anti-symmetric modes. The WT also demonstrates that the AE signal energy is not uniformly distributed between the modes that are present, nor is it uniformly distributed as a function of frequency along each of the dominant modes. These aspects demonstrate a key advantage of the WT as compared to an FFT. The WT shows how the signal energy is distributed as a function of frequency, time (or group velocity), and mode. In contrast, as is well known and illustrated in Fig. 3, the FFT of the same AE signal provides only the frequency content of the whole signal and does not allow one to easily see the modal division or how the intensity of the energy in particular frequency ranges and modes varies as a function of time (or group velocity). Thus, Fig. 2 shows that this AE source has the greatest concentration (most red color) of energy in the anti-symmetric fundamental mode in a frequency range of about 40 to 80 kHz over a range of group velocities from 1.8 to 2.7 mm/μs. Another large amplitude region of the WT is the part of the fundamental symmetric mode in a frequency range from about 500 to 540 kHz, which is centered about a group velocity of about 1.9 mm/μs. With regard to these frequency ranges and group velocities, we point out that the WT algorithm allows the user to select both the frequency resolution and the wavelet size. The effects on the WT results of different choices for these parameters are discussed next.

4. Parameter Selection to Enhance the Resolution/Smoothness of WT Results

The wavelet transform program, AGU-Vallen Wavelet, used in this research is that freely distributed on the World Wide Web (see web site www.vallen.de). There are several parameters that need to be selected prior to the wavelet calculation. Figure 4 shows the setup screen for this wavelet transform. Two parameters must be chosen properly to obtain sufficient resolution of the WT. These parameters are the "Frequency Resolution" and the "Wavelet size". The "Freq. Resolution" gives the frequency interval for the WT calculation, and has a default value of 10
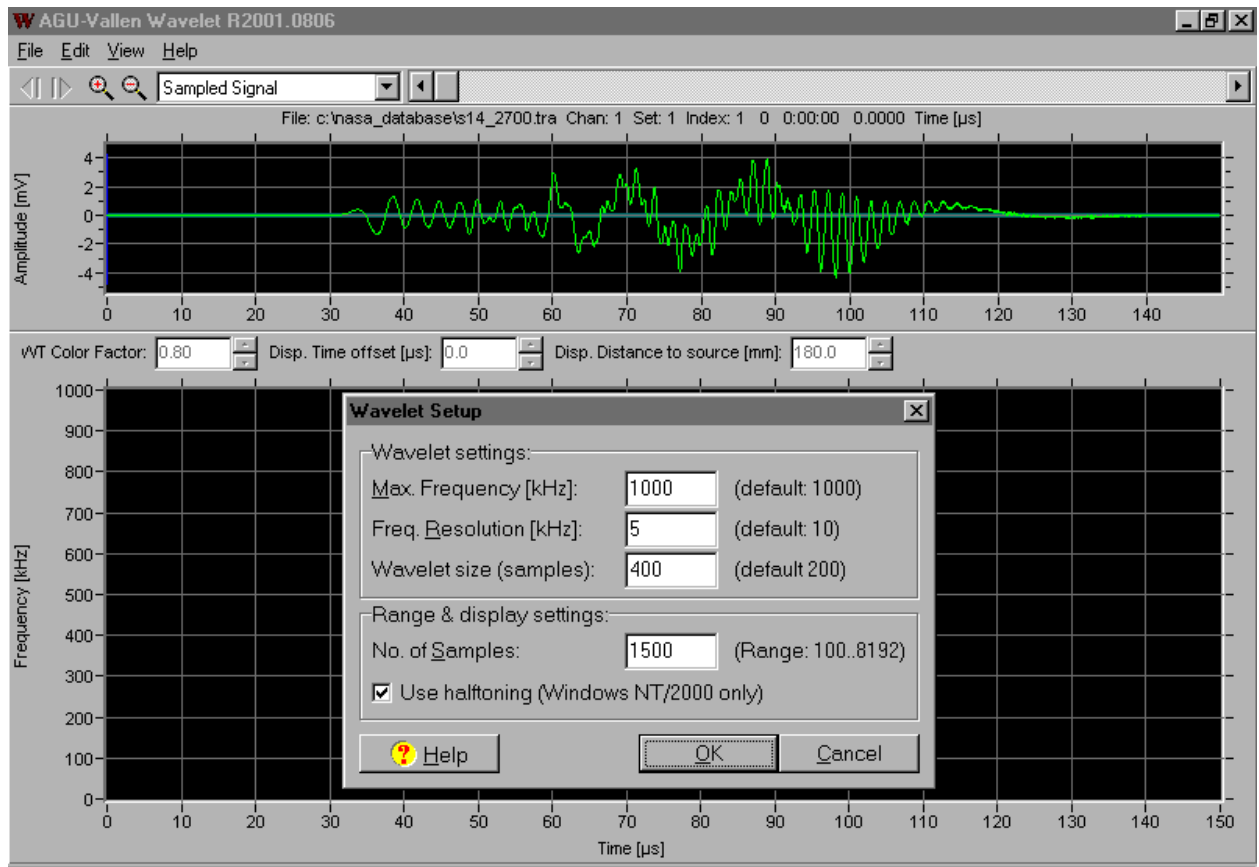
Fig. 4 "Wavelet Setup" screen for AGU-Vallen Wavelet.

kHz. This value is not necessarily the best, as is shown in Fig. 5. In this case the WT was calculated for an in-plane dipole centered at a depth of 0.47 mm in the large plate with a source-to-sensor propagation distance of 180 mm. Figure 5 (a) shows the WT result (CF = 1) with the default value of "Freq. Resolution" of 10 kHz and a "Wavelet size" of 800 samples, and Fig. 5 (b) shows the WT result (CF = 1) using a "Freq. Resolution" of 2 kHz and the same "Wavelet size". Clearly the 10 kHz frequency steps can be seen in Fig. 5 (a). These steps are not present in Fig. 5 (b), which shows a much smoother result. The disadvantage of using the smaller value for the frequency resolution is that the calculation takes longer. For example, on a personal computer with a CPU speed of 0.7 GHz, the WT shown in Fig. 5(a) took about 5 s and that shown in Fig. 5(b) took about 18 s.

The "Wavelet size" has a default value of 200 samples. Figure 6 shows the WT results of the same AE signal used for Fig. 5 with the default value (a) and a size value of 800 samples (b). For this figure the "Freq. Resolution" of 2 kHz was used along with a color factor of 1. It can be seen that the larger "Wavelet size" gives a smoother result. With a larger "Wavelet size" value, the calculation requires more time. To date, our observation has been that an increase in the "Wavelet size" is advisable when the larger amplitudes in the WT are at frequencies below about 100 kHz. Thus, we conclude that it is worthwhile to enhance the resolution and smoothness of the WT results at the cost of slightly longer computational times. For example, on a modern personal computer, the WT shown in Fig. 6 (a) took about 6 s and that shown in Fig. 6 (b) took about 18 s. When WT results were used to extract quantitative results, the parameters were selected to provide better resolution. In other cases lower resolution was used for more qualitative results.
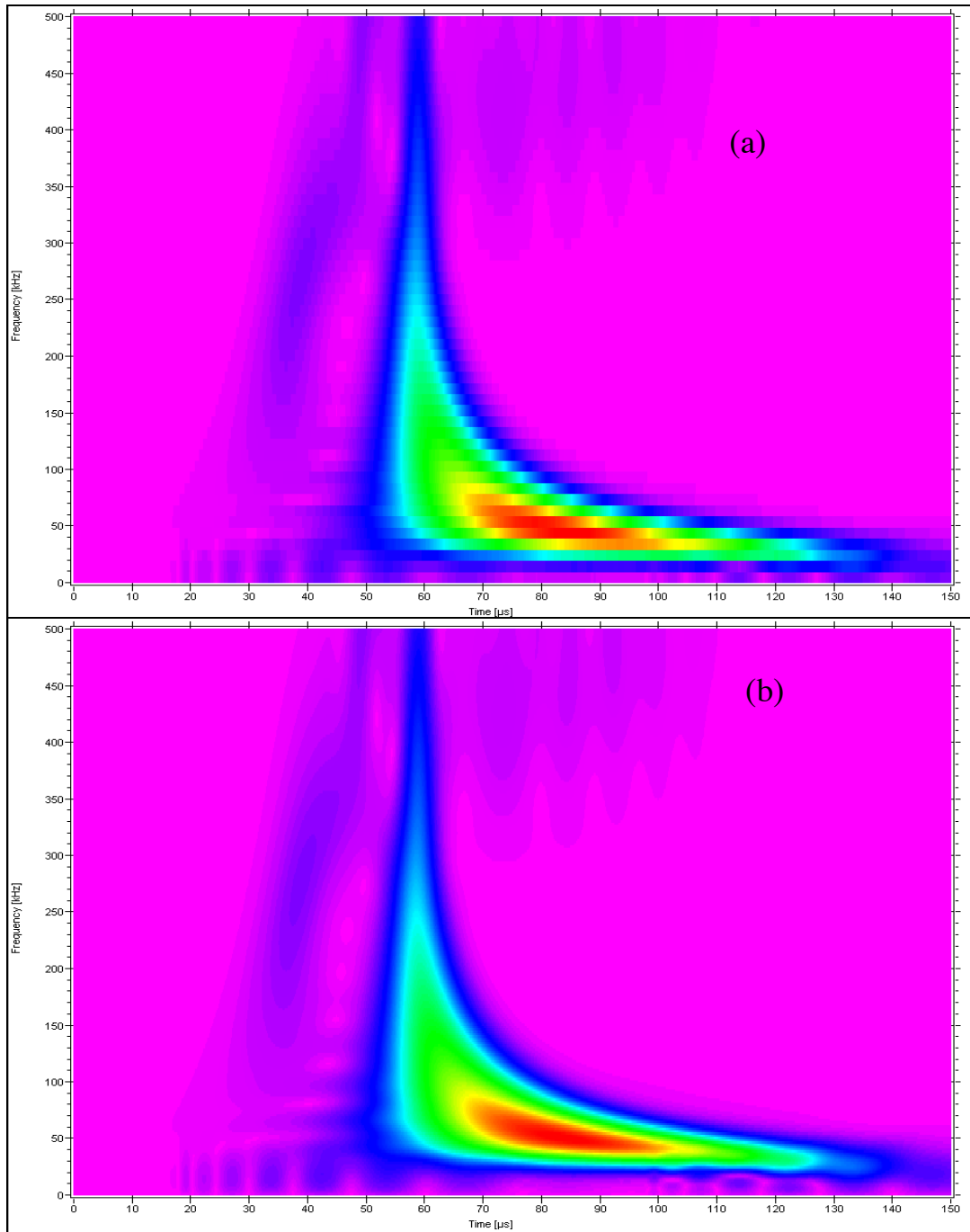
Fig. 5 WT results with low "Frequency resolution" (default) of 10 kHz (a) and high "Frequency resolution" of 2 kHz (b). Both results with a "Wavelet size" of 800 samples. Figures show frequency (0 to 500 kHz) versus time (0 to 150 μs).

5. Correlation of WTs with Source Type (Large Plate)

To begin to study source identification using the FEM database, we first focus on WT results of calculated AE signals at three different propagation distances from a single source. Figure 7 shows the WT results ("Freq. Resolution" of 2 kHz, "Wavelet size" of 600 samples and CF = 1) at the three available distances for an in-plane dipole source (dipole forces are aligned with the direction of propagation to the sensors) at a depth of 1.723 mm in a large plate. This figure
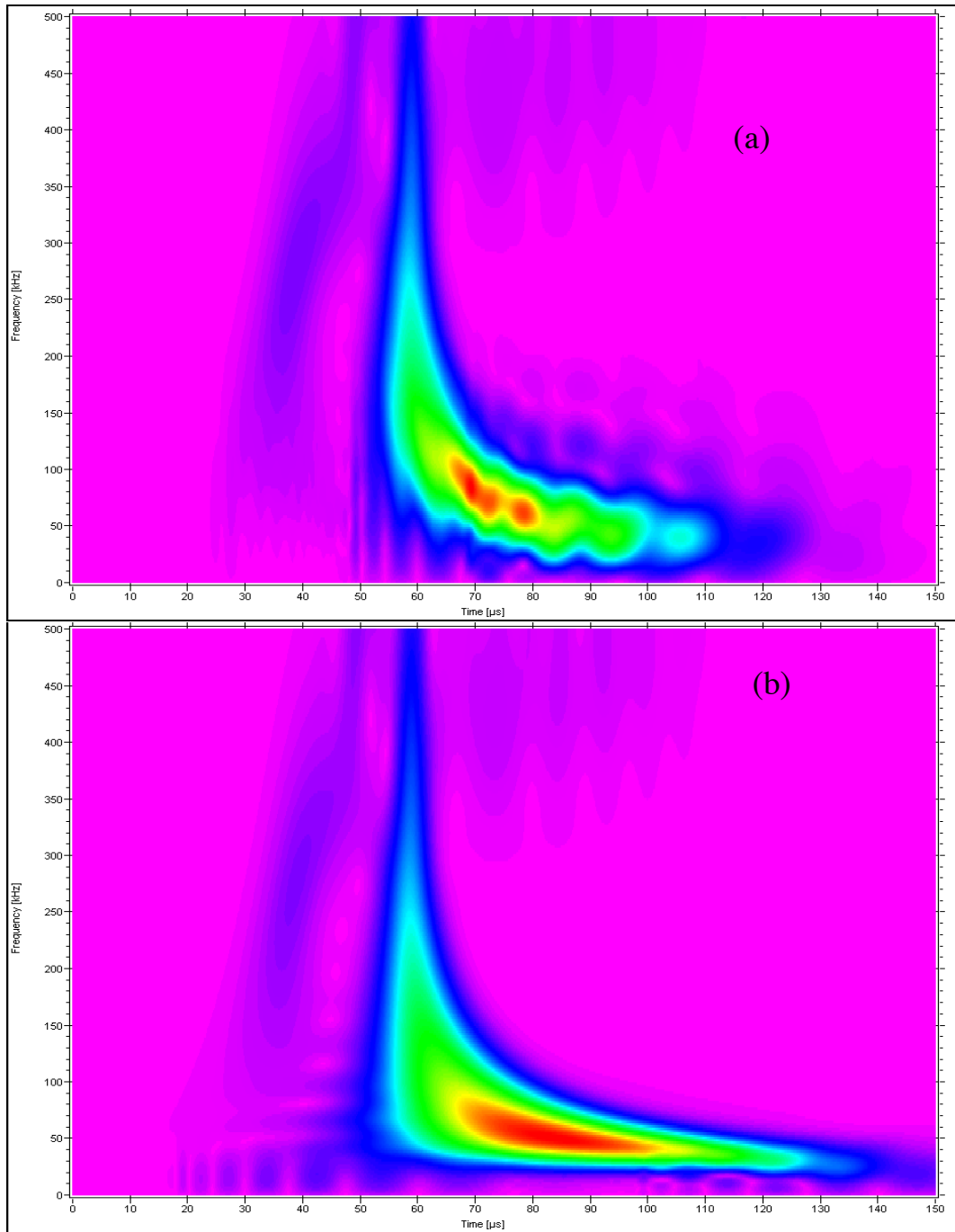
Fig. 6 WT results with small (default) "Wavelet size" of 200 samples (a) and large "Wavelet size" of 800 samples (b). Scales are the same as Fig. 5.

demonstrates that the WT results look very similar at different propagation distances when the time axis has been adjusted for the different distances. Due to this similarity with propagation distance, a limited data set could be extracted from the WT results that potentially shows that these three signals are from the same source. This potential was examined by extracting the WT peak magnitudes at two pairs of frequency and approximate group velocity. The frequencies and approximate group velocities were selected, one from each of the dominant WT magnitude regions of the fundamental modes. The circles in Fig. 7 show the two modal regions where the WT peak magnitudes and associated arrival times were extracted. The selected pairs of fre-
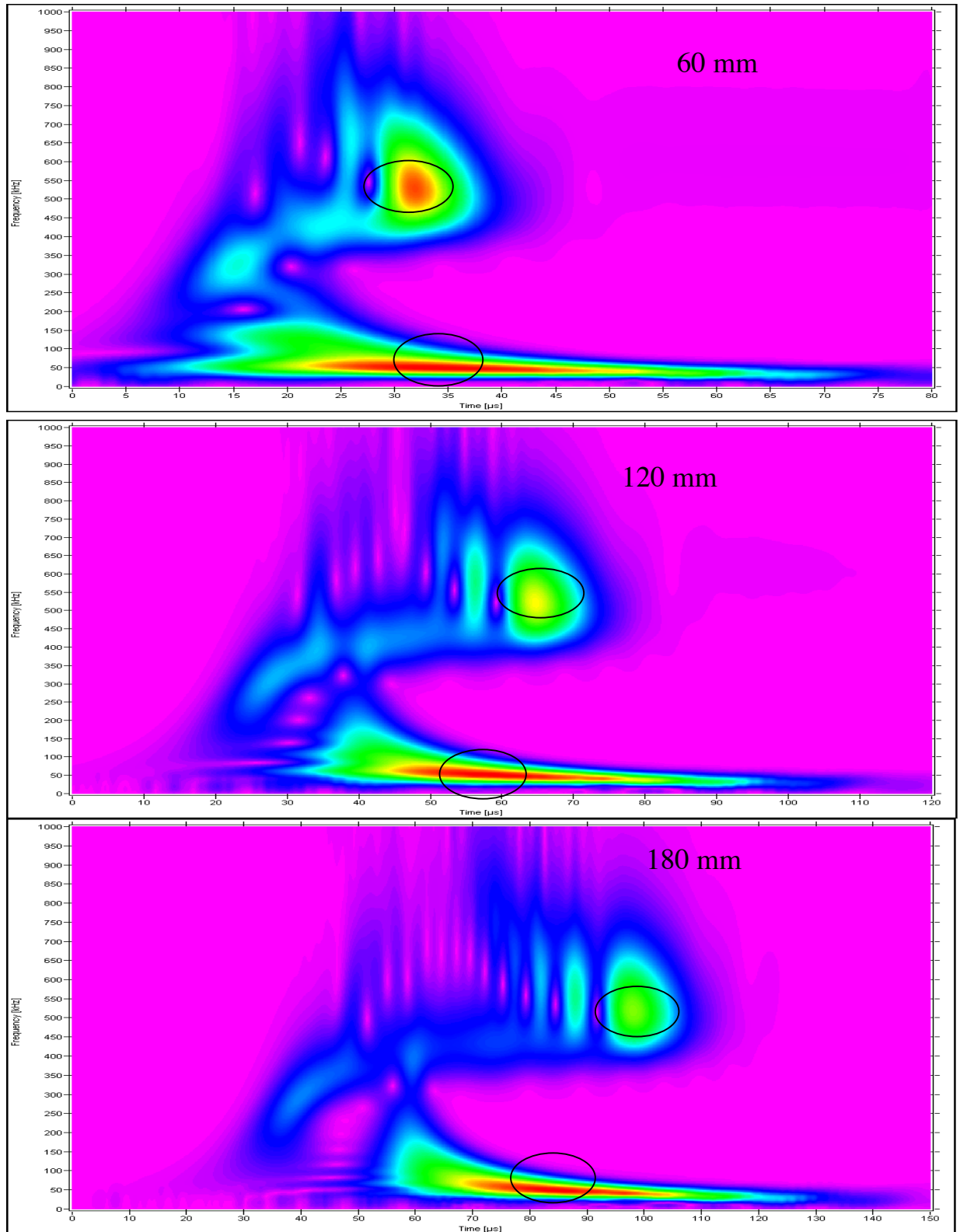
Fig. 7 WT results at three propagation distances 60 mm, 120 mm, and 180 mm for an in-plane dipole source at a depth of 1.723 mm. Circles show approximate regions from which the maximum WT magnitudes and group velocities were extracted at 50 kHz (Ao) and 522 kHz (So). Figures show frequency (0 to 1 MHz) versus time (0 to 80, 120, and 150 μs for the three propagation distances).

Table 1. WT magnitudes (peak value) for specified mode and frequency at indicated group velocity for in-plane dipole source at a depth of 1.723 mm.

Propagation distance, mm	Ao mode at 50 kHz		So mode at 522 kHz		Magnitude ratio, Ao/So
	Indicated group velocity, mm/μs	WT Magnitude	Indicated group velocity, mm/μs	WT Magnitude	
60	1.76	83,454	1.88	77,724	1.1
120	2.02	58,265	1.86	45,904	1.3
180	2.17	46,415	1.84	33,225	1.4

Table 2. WT magnitudes (peak value) for specified mode and frequency at indicated group velocity with sources at a depth of 1.723 mm and a propagation distance of 180 mm.

Source Type	Ao mode at 50 kHz		So mode at 522 kHz		Magnitude ratio, Ao/So
	Indicated group velocity, mm/μs	WT Magnitude	Indicated group velocity, mm/μs	WT Magnigude	
Out-of-plane	2.18	22,819	1.84	35,924	0.64
In-plane	2.17	46,415	1.84	33,225	1.4
Crack initiation	2.14	34,603	1.83	14,546	2.4

quency and group velocity were 50 kHz and about 2.16 mm/μs for the flexural mode (Ao) and 522 kHz and about 1.84 mm/μs for the extensional mode (So). The extraction of the peak WT magnitudes and their arrival times (in the approximate group-velocity region) was facilitated by an option that allows exporting the WT results into spreadsheets. Table 1 shows the extracted results. The indicated group velocity was obtained by dividing the extracted arrival time into the propagation distance from the source epicenter to the sensor location. Table 1 also shows the ratios of the Ao/So peak WT magnitudes at the selected frequencies and group velocities. The use of such a ratio provides a measure that is independent of the original source strength.

Although the Ao/So ratio experiences an increase with increasing propagation distance, this change could be corrected for by developing approximate rates of travel-distance attenuation of the WT magnitudes for the different modes and frequencies being used. Thus, it seems a limited set of data can be extracted (from WT results) that indicates the same source was observed at different propagation distances. However, it should be pointed out that the current dataset studies only the effect of propagation distance in one source-radiation direction (and the direction 180 degrees opposed; a symmetrical direction). Since a source in a plate emits different amounts of energy of the bulk modes in different radiation directions, future research should check the above conclusions (for source identification) when the propagation distance varies along with the two-dimensional radiation direction in the plane of the plate. Due to the typical symmetries of radiation patterns of sources aligned with the plate coordinate axes, this check will need to be done for only one quadrant rather than for a full 360 degrees.

To extend the study of extraction of a limited database for AE source identification from WT results, the next focus was on three different source types and their signals at a fixed propagation distance of 180 mm. Figure 8 shows (CF = 1) the WTs for an in-plane dipole (a), out-of-plane dipole (b), and a microcrack initiation (c) with all the sources centered at 1.723 mm below the top surface. These WTs were calculated with a "Frequency Resolution" (FR) of 2 kHz and a "Wavelet size" (WS) of 600 samples. Following the same procedure that was used with Fig. 7 to obtain the data in Table 1, the data shown in Table 2 were obtained from the WTs in Fig. 8. Again circles have been drawn in Fig. 8 about the regions from which the modes, approximate group velocities and frequencies were selected. Examination of Table 2 indicates that the sig-
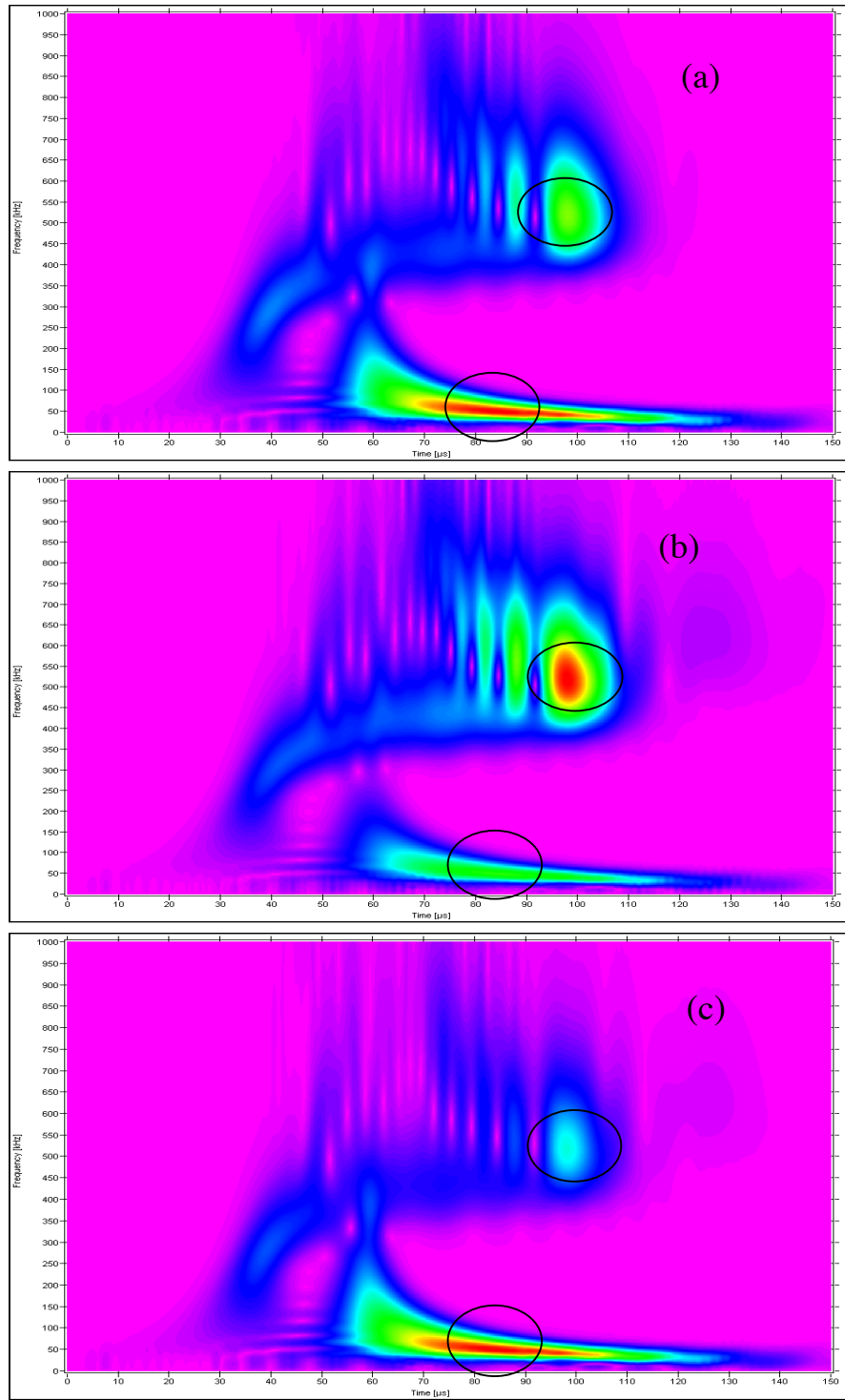
Fig. 8. WT results from out-of-plane displacement signals for three different source types: (a) in-plane dipole, (b) out-of-plane dipole and (c) crack initiation. Sources are all at a depth of 1.723 mm. Circles show approximate regions from which the maximum WT magnitudes and group velocities were extracted at 50 kHz (Ao) and 522 kHz (So). Figures show frequency (0 to 1 MHz) versus time (0 to 150 μs) for the signals at 180 mm propagation distance.

nificant changes of the simple Ao/So ratio potentially could be used for source identification. The out-of-plane dipole source had the smallest ratio, and the crack-initiation source had the largest ratio.
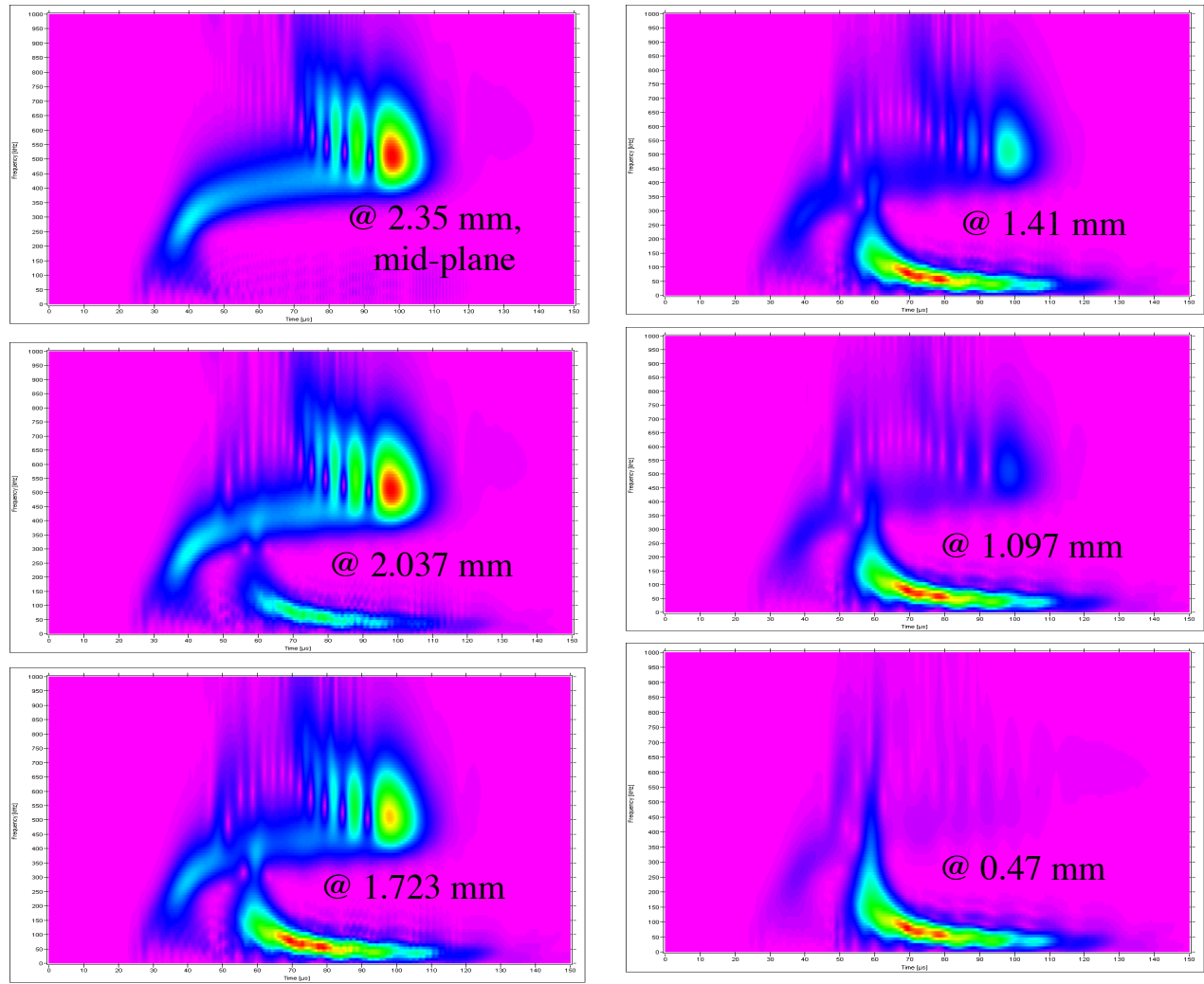
Fig. 9. WT plots as a function of the indicated source depths below the plate top surface. The source was an in-plane dipole with a 180 mm propagation distance. Figures show frequency (0 to 1 MHz) versus time (0 to 150 μs).

Examination of WT results for a single source type as a function of source depth reveals some potential difficulties in the approach suggested above. Figure 9 demonstrates the changes in WTs (with default values and CF = 1 for the AE signals at 180 mm) for an in-plane dipole as a function of the depth of the source below the top surface of the plate. Even a casual examination of the results in this figure shows that the WT result varies substantially as the depth of the source changes. For the source located at the mid-plane (at 2.35 mm) the fundamental symmetric (extensional) mode dominates. As the source is moved closer to the surface, it is clear that the energy carried in the extensional mode decreases and most of the energy is carried in the fundamental anti-symmetric (flexural) mode. This dependence of the dominant Lamb modes and associated frequencies can also be seen in the signal waveforms and their FFTs. These results are shown in Fig. 10 as a function of source depth for the same series of depths. The dependence of the WT results on source depth also is apparent for the out-of-plane dipole source and the more complicated microcrack initiation source. These WT results (default parameters and CF = 1) for the AE signals at 180 mm are shown in Fig. 11 for two different depths (0.783 and 1.723 mm).
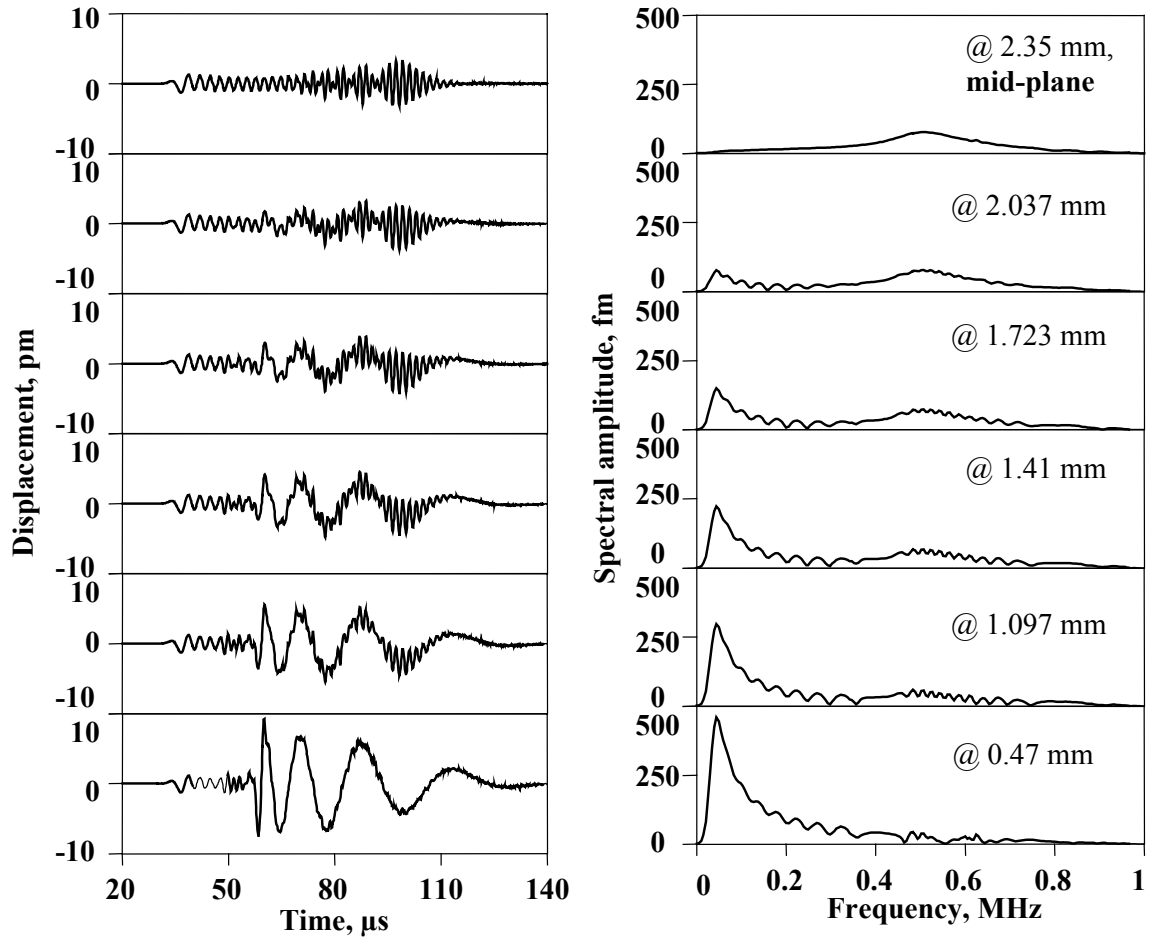
Fig. 10. Calculated AE signals with corresponding FFTs (in the same sequence top to bottom) for same cases shown in Fig. 9.

The possibility of extracting from WTs (of the out-of-plane displacement signals) a more limited data set to uniquely identify the different AE sources certainly exists. However, it is complicated by the dependence of the AE signals and their WTs on the depth of the sources. There are two primary reasons for this complication. First, the Ao/So ratio changes not just with source type but with source depth. The primary change (for the three source types considered) that takes place when the depth of a source changes is a transfer of more energy to either the ex-tensional mode or the flexural mode from the alternate mode. Thus, it does not seem possible to extract simple Ao/So ratio information, such as in Tables 1 and 2, from the WTs that is unique to a particular source type. Second, since at a fixed depth there are clear differences between source types (see Fig. 8 and Table 2), it is likely, as a consequence of the transfer of energy be-tween modes, that two different sources at two different source depths could have very similar WTs. This is in fact the case, as Figs. 12 and 13 show (calculated using default WT parameters) for signals at 180 mm from the sources. Figure 12 shows (CF = 1) that a microcrack initiation source (a) at a depth of 0.783 mm has nearly the same WT as an in-plane dipole source (b) at a depth of 0.47 mm. Figure 13 demonstrates (CF = 1) the close WT similarities between an out-of-plane dipole source (a) at a depth of 1.723 mm and an in-plane dipole source (b) at a depth of 2.037 mm.

Microcrack   **Out-of-plane dipole**

Source @ 0.783 mm deep
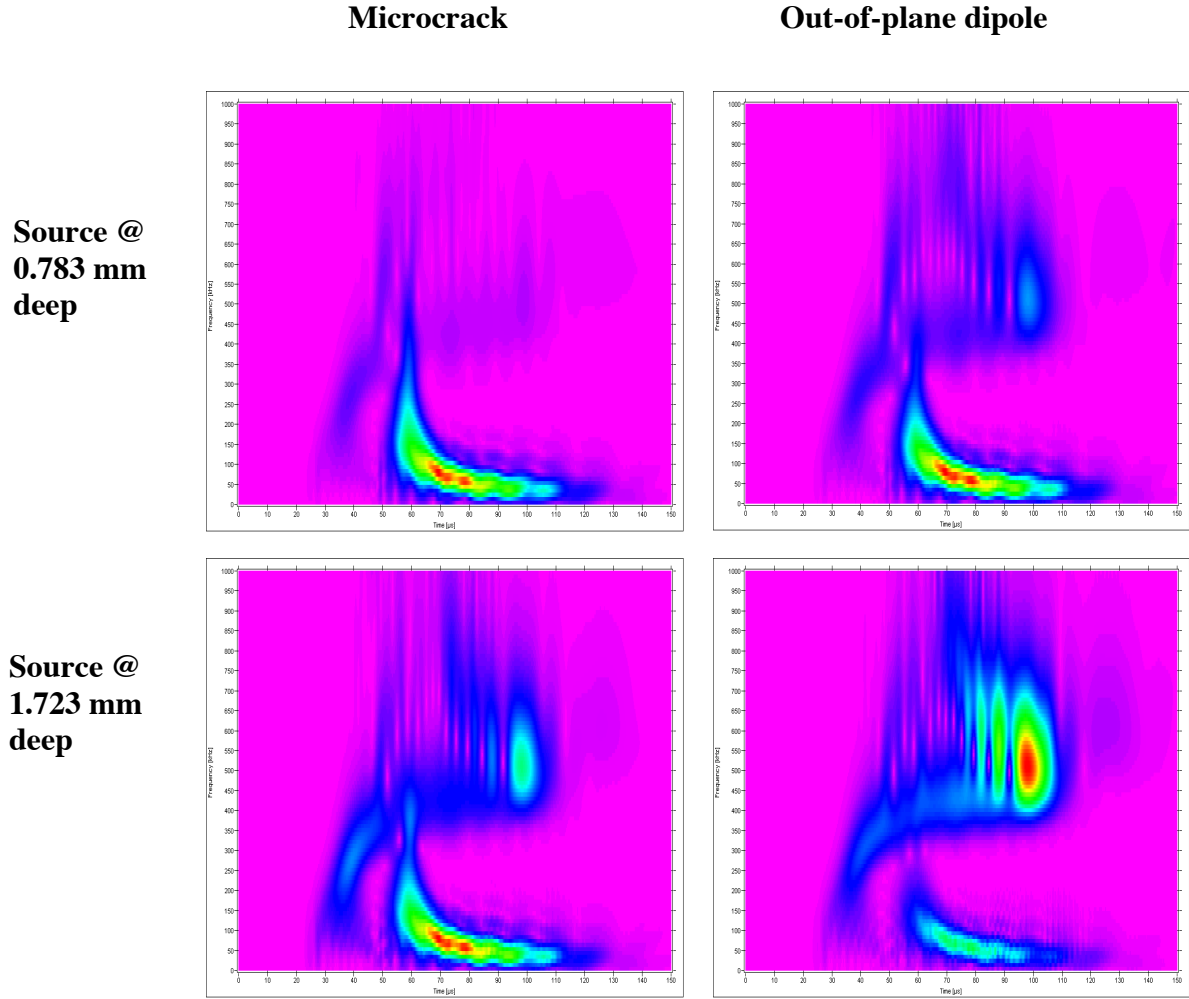

Source @ 1.723 mm deep

Fig. 11. WT plots showing the distinctions between a microcrack initiation source and an out-of-plane dipole compared at the same two different source depths and at 180 mm propagation distance. Plots show frequency (0 to 1 MHz) versus time (0 to 150 μs).

One might consider whether the lower-magnitude regions of the WTs in Figs. 12 and 13 might provide suitable simple features that would distinguish these sources. This might be the case as shown in Fig. 14, which shows WTs for the same signals used for Fig. 13 calculated with WS = 600 samples and FR = 2 kHz. Also in Fig. 14, the CF was set at 0.8 to provide a wider-magnitude range for the red color region. This setting of the CF effectively shows more features of the lower-magnitude parts of the WTs. The arrows in Fig. 14 point to regions where the WT of the in-plane dipole (b) has a larger magnitude than the WT of the out-of-plane dipole (a). But, this aspect that shows up very well in the FEM modeled data may not be nearly as clear when the typical signal-to-noise ratios of real AE signals are considered. In the modeled case, data has little or no apparent noise. Thus, examining differences in regions of lower WT magnitude may not be a practical solution for real AE signals.

To examine the depth effects more systematically and quantitatively, high-resolution WTs were calculated from signals at a propagation distance of 180 mm for the different source types and depths in the available database. The WT peak magnitudes at two pairs of frequency and approximate group velocity were then extracted for each case. The frequencies and approximate
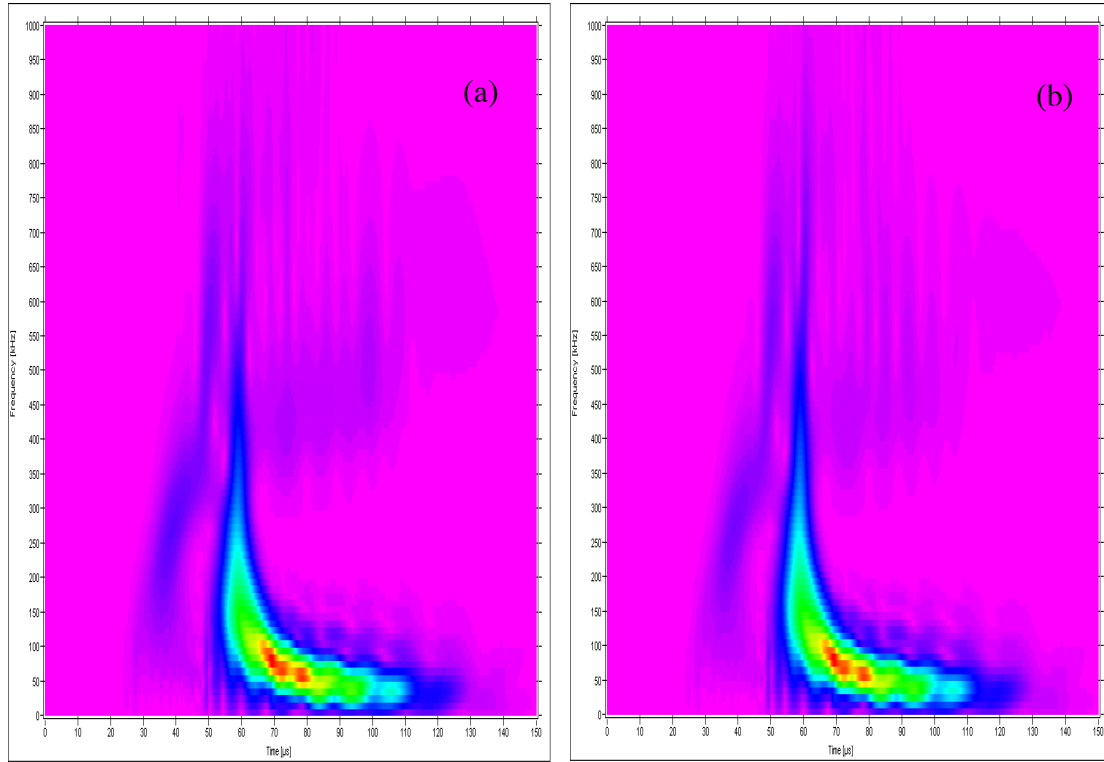
Fig. 12. WT plots showing the similarities for two different source types at different depths. At 180 mm propagation distance. Microcrack initiation (a) at 0.783 mm depth and in-plane dipole (b) at 0.470 mm depth. Plots show frequency (0 to 1 MHz) versus time (0 to 150 μs).
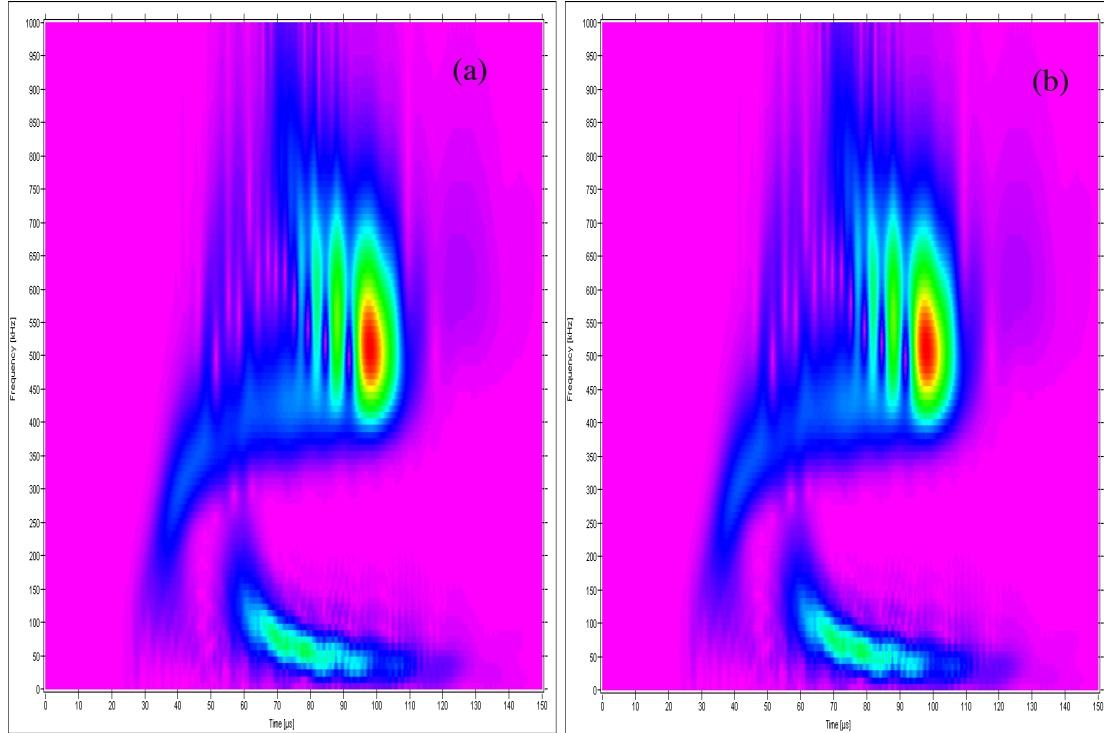

Fig. 13. WT plots show the similarities for two different source types at different depths. At 180 mm propagation distance. Out-of-plane dipole (a) at 1.723 mm depth and in-plane dipole (b) at 2.037 mm depth. Plots show frequency (0 to 1 MHz) versus time (0 to 150 μs).
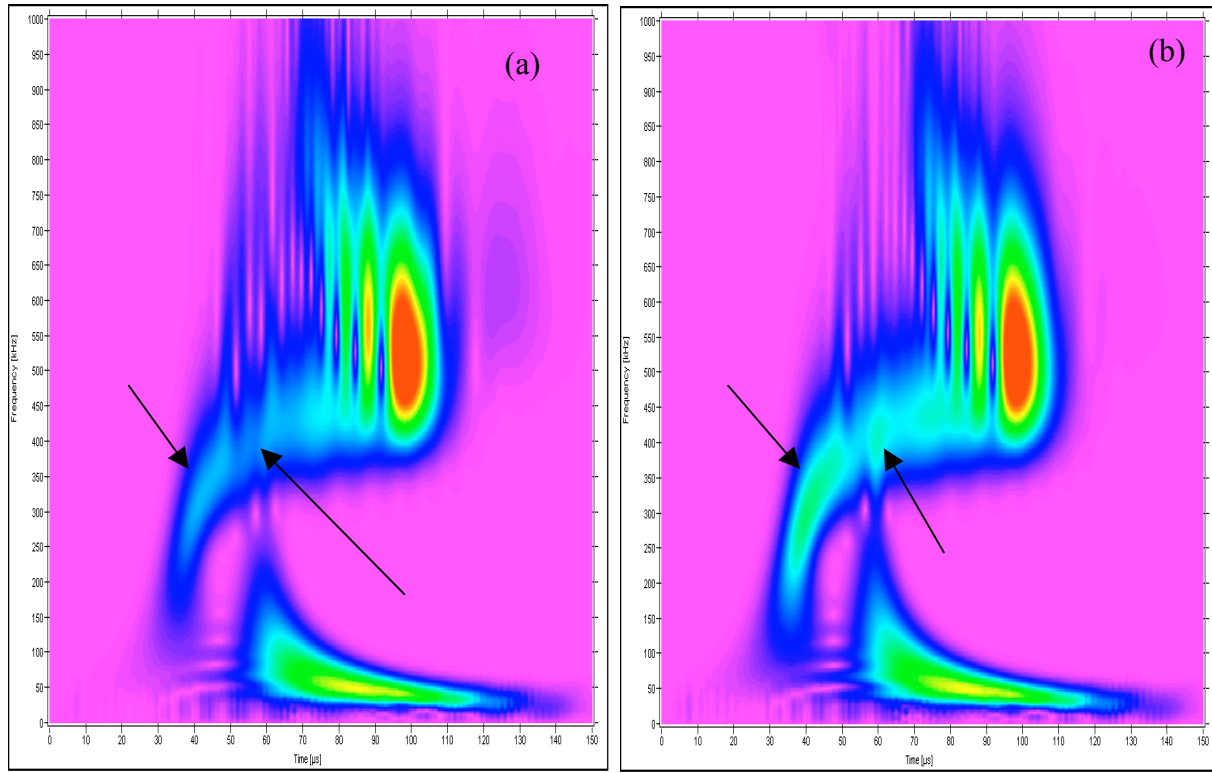
Fig. 14. Same cases and scales as Fig. 13 with color factor changed to 0.8 to examine differences in WTs in their lower magnitude regions. Arrows point to higher magnitude regions in the in-plane dipole (b) versus the out-of-plane dipole (a).
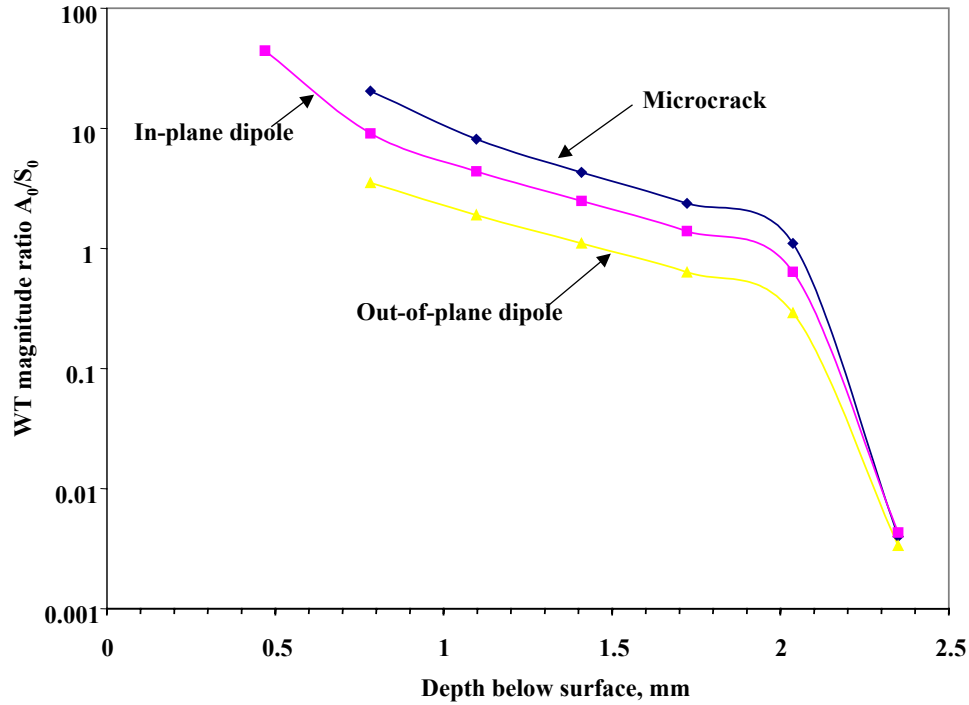

Fig. 15. Ao/So ratio of peak WT magnitudes versus AE source depth for the microcrack initiation, in-plane dipole and out-of-plane dipole sources at 180 mm propagation distance. Peak magnitudes at 50 kHz and approximate group velocity of 2.16 mm/µs for Ao and at 522 kHz and approximate group velocity of 1.84 mm/µs for So.

Table 3a. WT magnitudes (peak value) for specified mode and frequency at indicated group velocity for in-plane dipole source at 180 mm. (Note * indicates a peak was not present)

Source depth, mm	Ao mode at 50 kHz			So mode at 522 kHz			Magnitude ratio, Ao/So
	Indicated group velocity, mm/µs	WT Magnitude		Indicated group velocity, mm/µs	WT Magnitude		
2.35	2.18	160*		1.84	37,124		0.0043
2.037	2.18	23,104		1.84	36,138		0.64
1.723	2.17	46,415		1.84	33,225		1.4
1.41	2.14	70,427		1.84	28,398		2.5
1.097	2.14	95,209		1.83	21,738		4.4
0.783	2.14	121,144		1.83	13,331		9.1
0.47	2.15	148,578		1.82	3,357		44

Table 3b. WT magnitudes (peak value) for specified mode and frequency at indicated group velocity for microcrack initiation at 180 mm. (Note * indicates a peak was not present)

Source depth, mm	Ao mode at 50 kHz			So mode at 522 kHz			Magnitude ratio, Ao/So
	Indicated group veloicty, mm/µs	WT Magnitude		Indicated group velocity, mm/µs	WT Magnitude		
2.35	2.14	166*		1.84	16,535		0.004
2.037	2.14	17,248		1.84	16,035		1.1
1.723	2.14	34,603		1.83	14,546		2.4
1.41	2.18	52,296		1.83	12,084		4.3
1.097	2.14	70,490		1.83	8,669		8.1

Table 3c. WT magnitudes (peak value) for specified mode and frequency at indicated group velocity for out-of-plane dipole at 180 mm.

Source depth, mm	Ao mode at 50 kHz			So mode at 522 kHz			Magnitude ratio, Ao/So
	Indicated group velocity, mm/µs	WT Magnitude		Indicated group velocity, mm/µs	WT Magnitude		
2.35	2.16	132.7		1.84	39,605		0.0034
2.037	2.14	11,343		1.84	38,676		0.29
1.723	2.18	22,819		1.84	35,924		0.64
1.41	2.14	34,843		1.84	31,402		1.1
1.097	2.14	47,510		1.84	25,177		1.9
0.783	2.14	61,099		1.84	17,365		3.5

group velocities selected were those from the dominant WT magnitude regions of both fundamental modes. The selected values for the flexural mode (Ao) were 50 kHz and about 2.16 mm/µs. For the extensional mode (So), the values were 522 kHz and about 1.84 mm/µs. Then, as before, at each frequency the maximum WT magnitude and its arrival time were determined near the selected approximate group velocities. For certain cases the magnitudes of the WT are relatively small at the selected frequency and approximate group velocity, and in some cases the WT did not have a clear maximum in the approximate group-velocity region. In these latter cases, the WT magnitude at the selected frequency was selected at the same arrival time that the peak magnitude occurred when the same source type was at the nearest depth where the WT as a function of time had a true maximum in that region. The values determined are shown in Tables 3a, b and c for the three different source types. Also, these tables include the calculated magnitude ratio Ao/So for the range of source depths and source types. Figure 15 shows a plot of Ao/So versus source depth with the source type as a parameter. It is reasonable to conclude that there is a definite ordering of the Ao/So ratio as function of source depth. The microcrack initia-

tion source results in the highest values and the out-of-plane dipole has the lowest values, with the in-plane dipole source in between. The relative differences between the ratios at a fixed depth are not small, since the ratio scale in the figure is logarithmic. At the mid-plane depth (2.35 mm), the ratio values are likely not reliable due to the very small WT magnitudes for the Ao mode. Also, these Ao values were in most cases arbitrarily selected as described above since the Ao mode did not have a peak value for the approximate group velocity region of the mode.

It is clear in the case of experimental data when the source depth is unknown that the Ao/So ratio alone will not uniquely define a source type. But, if one considers the data in Fig. 15 to be that for a radiation direction of zero degrees, then it may be possible that results of Ao/So ratios from other radiation directions could provide sufficient additional information to uniquely identify the source type. This expectation, not unlike the approach of Buttle and Scruby (1990a), uses the fact that the radiation pattern is different for different source types. Since in experimental situations typically three or four sensors are hit when two-dimensional source location is determined (a prerequisite for the above approach, since the selected approximate group velocity needs to be converted to an approximate arrival time), signals are typically available in several two-dimensional radiation directions. For these different radiation directions, the Ao/So ratio could be extracted from WTs of the signals. These ratios could then be compared as a function of the radiation angle with modeled results of the Ao/So ratio versus radiation angle determined for different source types and depths. This method could possibly add sufficient information to uniquely identify the source type and source depth. Based upon these observations in future research we expect to examine the above approach with a FEM database that includes other radiation directions.

The application to experimental AE data of the Ao/So ratio approach will likely experience difficulties when the source is located very near the plate surfaces or very near the plate's mid-plane. As the first and last rows of Tables 3a, b and c show, in these cases either the Ao or So WT-based magnitude is small, and they do not always have a local maximum (at a given frequency and associated approximate group velocity). Thus, for experimental data from sources near the mid-plane, effects of low signal-to-noise ratios will likely eliminate the possibility of calculating meaningful Ao/So ratios. A possible solution to this problem might be to focus on the single dominant mode for these source-depth cases. For example, for a source located near or at the mid-plane of the plate two or more frequencies and associated approximate group velocities could be selected from the So mode. At these frequencies and velocities the maximum magnitudes of the WT could be determined within the So mode. Then ratios such as So (at 522 kHz) to So (at say 325 kHz) could be calculated. It is possible that this ratio or other appropriate ones might result in distinguishing different source types located near the plate mid-plane. And for a source located near the plate surfaces, a ratio from two frequencies of the Ao mode could be used. Hence, in future research we expect to examine such an approach using the current FEM database extended to include other source types, such as a shear source, and various radiation angles.

6. WT Data Subsets for Source Identification in Specimens with Nearby Edges

When the lateral size of the test specimen is decreased so that nearby edges are present, the AE signals and their WTs become much more complicated. This result is clearly seen in Fig. 16, which compares WTs of the AE signals (40 kHz high-pass) at 180 mm from in-plane and out-of-plane dipole sources in the small coupon specimen (Fig. 16(a)) and the large specimen (Fig. 16(b)) both at a depth of 1.723 mm. Figure 17(a) also shows as a function of propagation dis-

In-plane dipole   **Out-of-plane dipole**
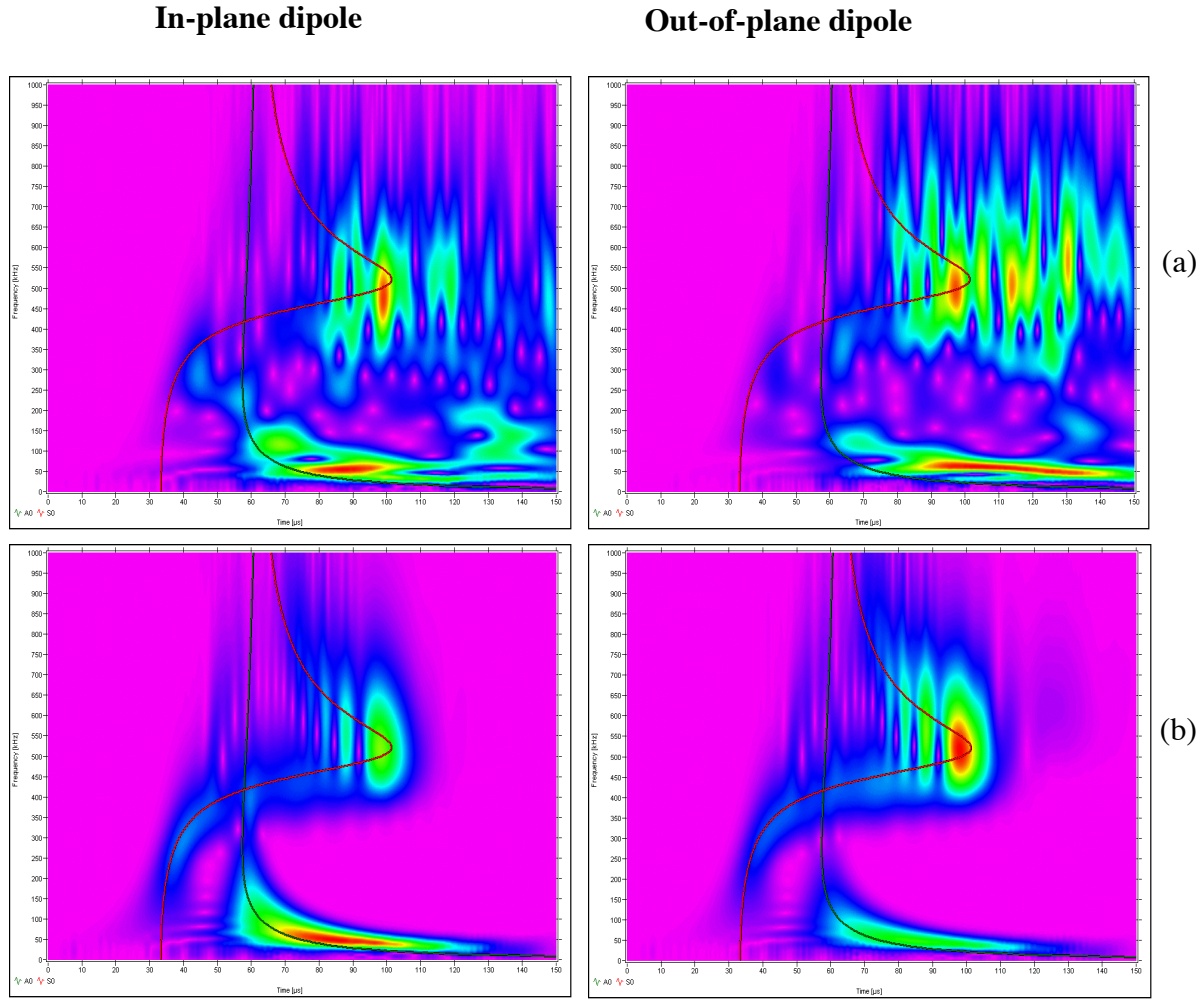

(a)

(b)

Fig. 16. WT results (40 kHz high-pass AE signals) for coupon specimen (a) with multiple edge reflections compared to large specimen (b) without edge reflections. Results shown for an in-plane dipole source and an out-of-plane dipole source with a propagation distance of 180 mm. Sources centered at 1.723 mm below the top surface of the plate. Frequency (0 to 1 MHz) versus time (0 to 150 μs). Superimposed fundamental modes shown.

tance the significant distortion in the WT results (of AE signals from an in-plane dipole) for the coupon specimen compared to the large specimen (Fig. 17(b)) with sources at a depth of 1.723 mm. The distribution of signal energy in the coupon as shown in Figs. 16(a) and 17(a) does not clearly follow the shapes of the superimposed fundamental Lamb-mode curves from the dispersion relations. Thus the extension of the possible extraction approaches proposed for source identification in the large plate is not straightforward for the coupon specimen. Further, since the distortion of the WT results is due to edge reflections (sides and at later times the specimen ends), moving the source from side-to-side across the 25.4 mm dimension of the coupon specimen will change the reflections in the AE signals. These source-position changes will also change the associated WTs as shown in Fig. 18 with superimposed fundamental modes. This figure compares the WTs for in-plane dipole sources as a function of the transverse position of the AE source. In Fig. 18(a), the source was located half-way across the specimen at 12.7 mm from the coupon side edge. In Figs. 18(b) and 18(c), the source was successively at 6.13 mm and 3.31 mm from the coupon side edge. The WTs (CF = 1, WS = 600) in these figures were calculated from the AE signals at 180 mm from the sources. The source depth was 2.35 mm. The
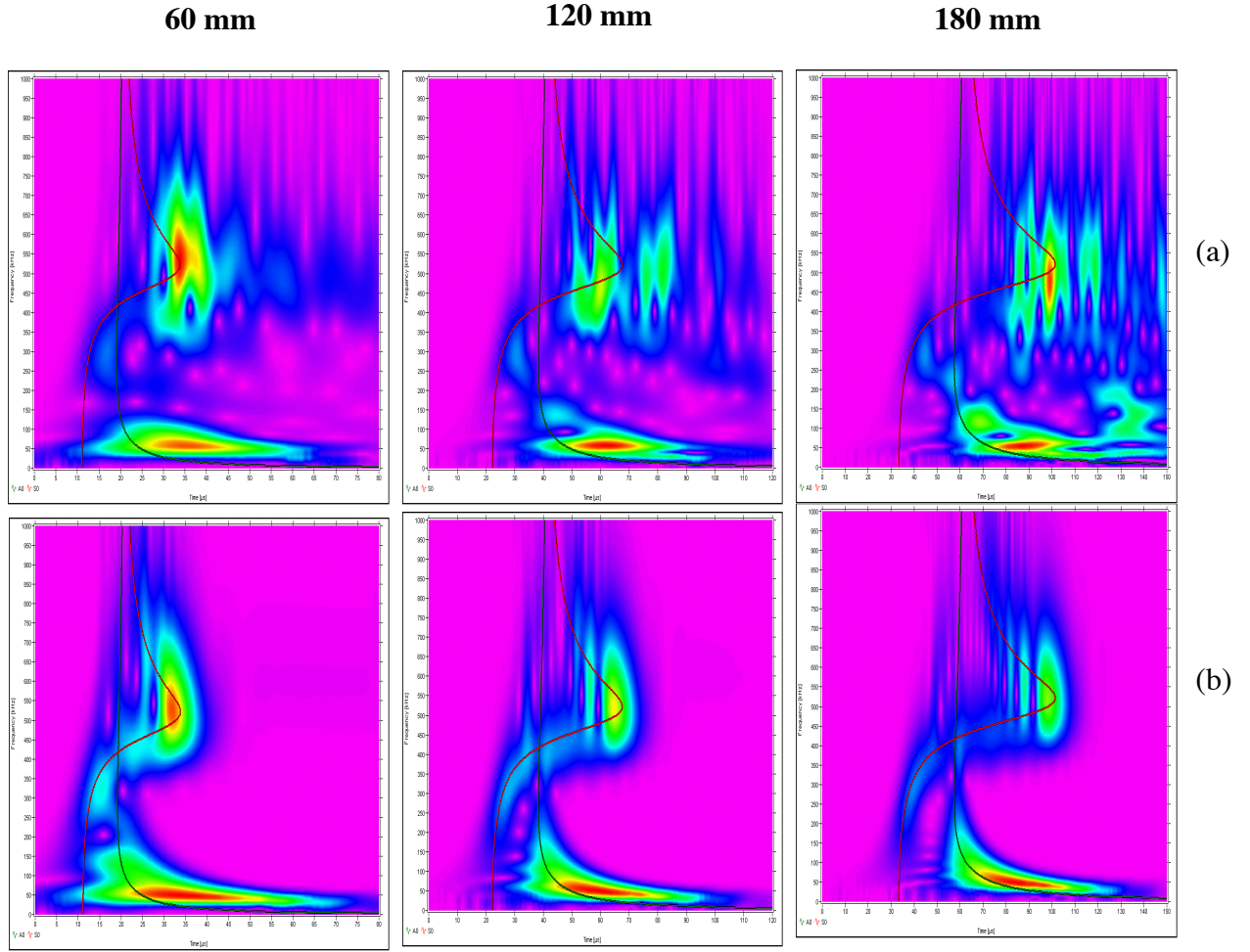
60 mm **120 mm** **180 mm**

(a)

(b)

Fig. 17. WT results (40 kHz high-pass AE signals) for coupon specimen (a) with multiple edge reflections contrasted to large specimen (b) without edge reflections at three propagation distances: 60 mm, 120 mm, and 180 mm. Source in-plane dipole centered at a depth of 1.723 mm below the top surface of the plate. Frequency (0 to 1 MHz) versus time (0 to 80, 120, and 150 μs with increasing propagation distance). Superimposed fundamental modes shown

current coupon database, except for the case illustrated in Fig. 18, does not include the side-to-side variation of the source position.

We believe the possible use of a WT for source identification in small specimens needs study because researchers use such specimens. Thus the necessary FEM database should be developed. But, it is prudent in the case of source identification that such studies be done after the potential difficulty of the dependence of the AE signals on the depth of the source is resolved. If the resolution of source depth difficulties requires the use of AE signals in several directions of radiation, then source identification in the small coupon specimen will likely require an alternate approach. This conclusion follows from the fact that in the coupon specimen far-field signals will not be available for different radiation directions. Researchers might be forced to use the bulk wave approach mentioned earlier (Buttle and Scruby, 1990a) if information from different propagation directions is required. This approach has been used in a 8-mm-thick coupon by placing the sensors in very close proximity to known crack tips (Buttle and Scruby, 1990b). Reducing the coupon thickness will eventually result in a sample that is too thin to allow one to
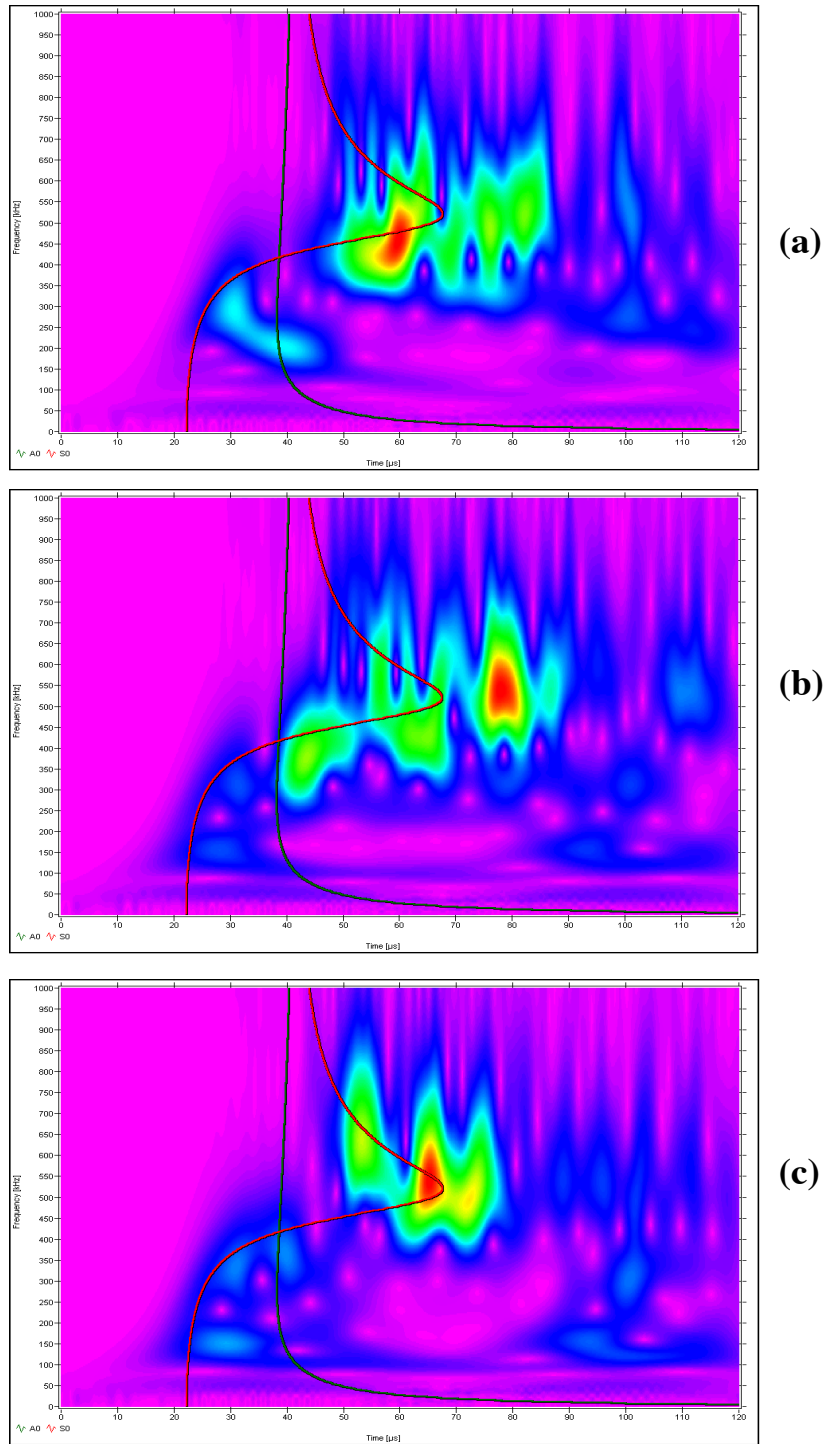
Fig. 18. Comparison of WT results (40 kHz high-pass AE signals) as a function of transverse position of the in-plane dipole source in the coupon specimen. The WTs with superimposed fundamental modes were calculated from the displacement signals at 120 mm for the mid-plane depth source. The sources were located half-way across the specimen (a) at 12.7 mm from the edge, (b) at 6.13 mm from the edge, and (c) at 3.31 mm from the edge. Plots show frequency (0 to 1 MHz) versus time (0 to 120 μs).

distinguish the bulk-wave arrivals from sample surface reflections. Also, to practice the bulk-wave approach, the AE sources of interest must be located in a small known region.

7. Conclusions

A. Source Identification–Large Plates

- For the 4.7 mm aluminum plate thickness of the current FEM database, a potentially useful parameter for source identification has been found. Using a separate selected frequency and approximate group velocity for each fundamental mode, the WT coefficients (usually local maxima for the frequency and group velocity) can be combined to form an Ao/So magnitude ratio. This ratio was found to distinguish different source types when the sources were all centered at the same depth below the plate surface and with the same propagation distance.
- But, since the values of this ratio overlap for different source types at different depths, it is not possible to uniquely identify the source type with this small set of WT-based data.
- The <u>current</u> database indicates that the value ranking of the Ao/So magnitude ratio for different source types remains in the <u>same</u> order as a function of source depth. Since this result is for a single radiation direction, it is to be expected that obtaining this ratio for other radiation directions will supplement the WT-based data with possibly sufficient information to uniquely classify the AE source type even with changing source depth. This expectation is based upon the fact that different source types have different AE-energy radiation patterns. Thus a series of WT-based magnitude ratios from a total number, n, of different radiation angles (e.g., $(Ao/So)_1$, $(Ao/So)_2$, …, $(Ao/So)_n$) could form an input vector to an artificial intelligence (AI) software program that would determine the AE source type. The AI program could be initially trained using a FEM-generated database.

B. Source Identification–Small Coupon Specimens

- The inherent multiple edge reflections present in small coupon specimens complicate the use of WT coefficients for source identification. Since the current small coupon FEM database does not include (except for one case) the important parameter (relative to edge reflection effects) of changes in specimen side-to-side position of the source, the current database did not allow a full examination of these complications.

References

D. J. Buttle and C. B. Scruby, "Characterization of Fatigue of Aluminum Alloys by Acoustic Emission, Part 1-Identification of Source Mechanism", Journal of Acoustic Emission, **9**, No. 4, 1990a, 243-254.

D. J. Buttle and C. B. Scruby, "Characterization of Fatigue of Aluminum Alloys by Acoustic Emission, Part II – Discrimination Between Primary and Secondary Emissions", Journal of Acoustic Emission, **9**, No. 4, 1990b, 255-269.

Dawei Guo, Ajit K. Mal and Marvin A. Hamstad, "AE Wavefield Calculations in a Plate", in *Progress in Acoustic Emission IX*, Acoustic Emission Working Group and Acoustic Emission Group, 1998, pp. IV-19 to IV-29.

M. A. Hamstad, A. O'Gallagher and J. Gary, "Modeling of Buried Acoustic Emission Monopole and Dipole Sources With a Finite Element Technique", Journal of Acoustic Emission, **17**, No. 3-4, 1999, 97-110.

R. L. Mehan and J.V. Mullin, "Analysis of Composite Failure Mechanisms Using Acoustic Emissions", Journal of Composite Materials, **5**, April 1971, 266-269.

W. H. Prosser, M. A. Hamstad, J. Gary and A. O'Gallagher, "Reflections of AE Waves in Finite Plates: Finite Element Modeling and Experimental Measurements", Journal of Acoustic Emission, **17**, No. 1-2, 1999, 37-47.

H. Suzuki, T. Kinjo, Y. Hayashi, M. Takemoto and K. Ono, "Wavelet Transform of Acoustic Emission Signals", Journal of Acoustic Emission, **14**, No. 2, 1996, 69-84.

M. Takemoto, H. Nishino and K. Ono, "Wavelet Transform - Applications to AE Signal Analysis", Acoustic Emission - Beyond the Millennium, Elsevier (2000), pp. 35-56.

Vallen-Systeme GmbH, München, Germany, http://www.vallen.de/wavelet/index.html, 2001.

R. Weaver and Y. H. Pao, "Axisymmetrical Waves Excited by a Point Source in a Plate", Journal of Applied Mechanics, **49**, 1982a, 821-836.

R. Weaver and Y. H. Pao, "Spectra of Transient Waves in Elastic Plates", Journal of the Acoustical Society of America, **72**, 1982b, 1933-1941.

H. Yamada, Y. Mizutani, H. Nishino, M. Takemoto and K. Ono, "Lamb Wave Source Location of Impact on Anisotropic Plates", Journal of Acoustic Emission, **18**, (2000, December), 51-60.